

Title	Order-Disorder Phenomena and Their Effects on Bandgap in ZnSnP
Author(s)	Nakatsuka, Shigeru; Nose, Yoshitaro
Citation	The Journal of Physical Chemistry C (2017), 121(2): 1040-1046
Issue Date	2017-01-19
URL	http://hdl.handle.net/2433/243843
Right	This document is the Accepted Manuscript version of a Published Work that appeared in final form in The Journal of Physical Chemistry C, copyright © American Chemical Society after peer review and technical editing by the publisher. To access the final edited and published work see https://doi.org/10.1021/acs.jpcc.6b11215 .; This is not the published version. Please cite only the published version. この論文は出版社版ではありません。引用の際には出版社版をご確認ご利用ください。
Type	Journal Article
Textversion	author

Order-disorder phenomena and their effects on bandgap in ZnSnP₂

Shigeru Nakatsuka and Yoshitaro Nose

Department of Materials Science and Engineering, Kyoto University, Kyoto 606-8501,
Japan.

Keywords: order-disorder, bandgap, order parameter, Rietveld refinement

Abstract

A ternary compound semiconductor ZnSnP₂ has the order-disorder transition, where the ordered and disordered phases are chalcopyrite ($I\bar{4}2d$, $a = 5.651 \text{ \AA}$, $c = 2a$) and sphalerite ($F\bar{4}3m$, $a = 5.651 \text{ \AA}$), respectively. In this study, the quantitative relationship between bandgap and long-range order parameter η was investigated by analyzing the ZnSnP₂ bulk crystals obtained at various cooling rates. The Chipman and Warren method was used to evaluate XRD profiles and we determined the long-range order parameter in ZnSnP₂ crystal. The results showed that the long-range order parameter η decreases from 0.94 to 0.54 with the increase of cooling rates, and the bandgap gradually reduced from 1.60 to 1.37 eV, corresponding to the η value. It was also demonstrated that bandgap tuning of ZnSnP₂ is possible by controlling the long-range order parameter using annealing process. This study clarified the effects of the order-disorder phenomena on bandgap in ZnSnP₂ as a model material through the evaluation of long-range order

parameter, which is also a promising technique to tune the bandgap without composition control.

To whom all correspondence should be addressed. Tel.: +81-75-753-5472; Fax: +81-75-753-3579; E-mail: nose.yoshitaro.5e@kyoto-u.ac.jp.

1. Introduction

Bandgap of semiconductors is one of the most important properties for optoelectric devices, and it is controlled in order to achieve an intended device efficiency. For example, $\text{CuIn}_{1-x}\text{Ga}_x\text{Se}_2$ is a solar absorber for photovoltaics, and the bandgap can be controlled by adjusting the molar ratio of In and Ga. In a practical case, the bandgap of $\text{Cu}_{1-x}\text{In}_x\text{GaSe}_2$ is tuned to 1.2 eV using the solid solution between CuInSe_2 and CuGaSe_2 , which have bandgaps of about 1.0 and 1.7 eV, respectively.¹ In a further example, bandgap tuning in a multi-junction solar cell with the structure $\text{In}_x\text{Ga}_{1-x}\text{P}/\text{GaAs}/\text{Ge}$, is achieved by using the solid solution between InP and GaP.²

It is also observed that bandgap changes can occur due to phase transitions. An order-disorder transition is a structural phase transition without composition change. In some ternary compounds such as CuInSe_2 ³ and CuInS_2 ⁴, it was reported that the crystal structure varied between chalcopyrite and sphalerite due to the order-disorder transition. Therefore, it was considered that bandgap tuning could be achieved using order-disorder transitions, without requiring composition change.

A ternary compound semiconductor ZnSnP_2 with chalcopyrite structure shows p-type conductivity due to intrinsic defects,⁵ and has a direct bandgap of 1.66 eV.⁶ Bandgap tuning using the solid solution between ZnSnP_2 and CdSnP_2 was proposed based on first principle calculations.⁷ In addition, an order-disorder transition was also suggested in ZnSnP_2 with a transition temperature, T_c , of about 720 °C, determined by differential

thermal analysis⁸ ; however, in-situ high temperature X-ray diffraction, as reported for CuInSe₂,³ was not performed on ZnSnP₂ and T_c has not been precisely evaluated. In this transition, the ordered and disordered phases are chalcopyrite ($I\bar{4}2d$, $a = 5.651 \text{ \AA}$, $c = 2a$) and sphalerite ($F\bar{4}3m$, $a = 5.651 \text{ \AA}$), respectively,⁶ as shown in Figure 1. In the disordered state, Zn and Sn cations occupy their sites randomly, while the sublattice of phosphorus is maintained. First principle calculations suggest that the bandgaps of ZnSnP₂ with chalcopyrite and sphalerite structures are 1.70 and 0.75 eV, respectively.⁹

In the case of the growth of ZnSnP₂ thin film on GaAs (100) by gas source molecular beam epitaxy, it was reported that the structure of ZnSnP₂ can be controlled by tuning the flux ratio of Zn and Sn.¹⁰ When the flux ratio of Zn/Sn was 0.26 at a substrate temperature of 350 °C, superlattice reflections were observed in the XRD profiles. For a flux ratio of Zn/Sn = 0.22, only fundamental reflections were observed, which meant that a ZnSnP₂ thin film with sphalerite structure was formed.¹¹ Francoeur *et al.* evaluated the long-range order parameter η , which is an index indicating the degree of ordering, from XRD profiles in ZnSnP₂ thin films grown on GaAs (100) substrates.¹⁰ They reported that the long-range order parameter of ZnSnP₂ changed from 0 to 0.3, depending on the flux ratio Zn/Sn.¹² In order to determine the bandgap of ZnSnP₂, St-Jean *et al.* performed electroreflectance measurements for ZnSnP₂ thin films grown epitaxially on GaAs (100).¹³ The bandgap of ZnSnP₂ with $\eta = 0$, which corresponds to the sphalerite structure, was determined to be 1.383 eV. Two optical transitions at 1.381 and 1.683 eV were observed in the

electroreflectance spectrum of ZnSnP_2 with $\eta=0.3$. The ZnSnP_2 bandgaps at 1.381 and 1.683 eV were considered to be derived from the sphalerite and perfectly-ordered chalcopyrite structures, respectively. They concluded that ZnSnP_2 with $\eta = 0.3$ is composed of perfectly-ordered domains and a disordered matrix.

In an order-disorder transition, thermodynamic equilibrium of perfectly-ordered and disordered phases cannot be achieved. St-Jean *et al.* considered the microstructure of ZnSnP_2 based solely on the value of the bandgap, however, the microstructure should be correctly investigated using XRD analysis and observation by microscope. In the study on CuInSe_2 by Shorror *et al.*,³ the phase transition between chalcopyrite and sphalerite was assumed to be a first-order transition, and it is therefore difficult to consider that a relatively low long-range order parameter is not thermodynamically achieved, as in the case of $\eta = 0.3$. Based on the findings of these reports, it is necessary to precisely evaluate the value of η and quantitatively investigate its relationship with bandgap in order to understand the reported phenomena.

It has also been reported that the bandgap of ZnSnP_2 is related to the growth conditions in bulk crystals. The peak intensities of superlattice reflections in XRD profiles decreases with the increase of the cooling rate in crystals grown by the flux method.^{14, 15} The experimental results imply that an increase of the cooling rate leads to cation disordering. From photoelectrochemical measurements, the bandgaps of ZnSnP_2 bulk crystals with chalcopyrite and sphalerite structure were found to be 1.64 and 1.25 eV, respectively.¹⁵

However, the corresponding relationship between bandgap and atomic arrangement has not been sufficiently discussed.

As described above, the bandgap in ZnSnP_2 bulk crystals seems to change due to the order-disorder transition. In this work, we thus precisely evaluated the long-range order parameter and investigated a quantitative relationship between bandgap and long-range order parameter using bulk crystals in order to clarify this phenomena. In addition, it is considered that the bandgap has a temperature-dependence if it depends on the order parameter. Consequently, the impact of temperature on bandgap was investigated by annealing experiments.

2. Experimental methods

ZnSnP₂ crystals were grown by the flux method described in our previous work.¹⁶ The raw materials, Zn shot (99.99%, Kojundo Chemical Laboratory), Sn shot (99.99%, Kojundo Chemical Laboratory) and red phosphorus flake (99.9999%, Kojundo Chemical Laboratory) were sealed in evacuated quartz ampoules. The ampoules were then placed in a growth furnace and homogenized at 700 °C. The furnace was raised and the samples were unidirectionally solidified from the bottom. In this study, the crystal growth of ZnSnP₂ was carried out with varied cooling rates (0.7, 15, 50, 200 and 640 °C/h). For the samples prepared with the cooling rate of 0.7 °C/h, the crystals grown at the bottom of the samples were cut into several plates and ground by mortar and pestle into a fine powder for evaluation. For the samples with the other cooling rates, the crystals were sparsely precipitated in Sn flux. In these samples, the crystals were extracted by dissolving the Sn flux in a solution of 10 M HNO₃ and 1 M NaCl and formed into powder. To anneal the crystals, powder samples were formed into pellets by uniaxial compression at 80 MPa and then sealed in evacuated quartz ampoules under a pressure of 10⁻² Pa. The samples were then heated at various temperatures for a week and finally quenched to room temperature.

The product phases were identified by X-ray diffraction (XRD, Panalytical X'Pert Pro Alpha-1), where CuKα₁ ($\lambda = 1.5406 \text{ \AA}$) was used as an X-ray source (45 kV, 40 mA). The order parameter in ZnSnP₂ crystals was evaluated from the peak area ratio of the

superlattice to fundamental reflections. Rietveld refinement of the XRD profiles was also carried out using the RIETAN-FP¹⁷ in order to evaluate the order parameter from the other viewpoint. The bandgap of the crystals was evaluated from the diffuse reflectance spectra of powder samples measured by a spectrophotometer (SHIMAZU UV-2600). The composition of crystals was measured by Inductively-Coupled Plasma Atomic Emission Spectrometry (ICP-AES) using an ICP Optical Emission Spectrometer (SII Nano Technology, SPS3520UV).

3. Results and discussion

3.1. Influence of cooling rate on ordering behavior

Table 1 shows the composition of the crystals grown with the different cooling rates. The composition of each sample is close to the stoichiometric ratio of ZnSnP_2 and is independent of the cooling rate. Figure 2 shows the XRD profiles of the ZnSnP_2 crystals grown by the various cooling rates. The diamond and triangle symbols indicate the reference patterns of ZnSnP_2 with chalcopyrite and sphalerite structures, respectively. The reflections identified by the diamond symbols alone correspond to superlattice reflections and those identified by both symbols are fundamental reflections. The profiles and reference patterns are normalized by the intensity of (112) diffraction peaks, and the indices for the chalcopyrite structure are shown in the figure.

Figure 2a shows that single phase ZnSnP_2 was obtained in all samples. In spite of the almost identical compositions of the crystals, the peak intensity of the superlattice reflections, such as (101), decreases with the increase of cooling rate, as shown in Figure 2b. This might indicate a decrease of the degree of ordering in ZnSnP_2 crystals. In addition, the FWHM of the superlattice reflection peaks became larger with the increase of the cooling rate, while that of fundamental peaks seemed to be independent of the cooling rate. Zn and Sn layers stack alternately in the [101] direction, therefore, it is thought that the disordering of Zn and Sn atoms results in modified distribution of the spacing of the planes, which in turn leads to broadening of (101) superlattice reflections. On the other

hand, the (112) plane consists of the same number of Zn and Sn atoms on average, in both ordered and disordered structures, and it is assumed that the effect of the disordering on (112) diffraction is small.

In this study, the degree of ordering in ZnSnP₂ was evaluated using the Chipman and Warren method.¹⁸ Here, we focused on the Zn-Sn sublattice in ZnSnP₂. The Bragg-Williams long-range order parameter η is defined as $\eta = r_{\alpha}^{\text{Zn}} + r_{\beta}^{\text{Sn}} - 1$, where α and β represent the sites occupied by Zn and Sn in perfectly-ordered chalcopyrite structure, respectively, and r_i^j means the occupancy of i sites occupied by j atoms. The order parameter was experimentally evaluated by the peak area ratio of superlattice to fundamental reflections. In this study, (101) diffraction and (112) or (200) (004) diffractions were adopted as the superlattice and fundamental reflections, respectively. The peak area intensity of an hkl reflection, A_{hkl} , is represented by the following equation, using multiplicity m_{hkl} , Lorentz-polarization factor LP_{hkl} , structure factor, F_{hkl} , and Debye-Waller factor, $\exp(-2M)$.¹⁸

$$A_{hkl} = C \cdot m_{hkl} \cdot LP_{hkl} \cdot |F_{hkl}|^2 \exp(-2M), \quad (1)$$

where C is the constant containing an absorption factor. The structure factor, F_{hkl} , was calculated for the various long-range order parameters using VESTA.¹⁹ Lattice constants of $a = 5.651$ and $c = 11.302 \text{ \AA}$ ⁶ were used and an anion displacement parameter u , which was 0.239¹⁴ in this study, was used for a tetrahedral distortion in chalcopyrite structure. The atomic scattering factors are correction terms for dispersion.^{20, 21} In this study, they

were taken from the paper reported by D. Waasmaier *et al.*²² For the isotropic temperature factors necessary to the calculation of the Debye-Waller factor, we used the values evaluated from first principles.²³ The peak area ratios of the superlattice to fundamental reflections, A_{101}/A_{112} and $A_{101}/A_{200\ 004}$, as the function of η value, were calculated using equation (1), and the results are shown in [Figure 3](#). The long-range order parameter η of each sample was evaluated by comparing the experimental ratio with the calculated value. For the evaluation of area intensities, each diffraction peak was fitted using the Voigt function.

Rietveld refinement of XRD profiles was also carried out. The values of refined parameters are summarized in [Table 2](#). The long-range order parameter was calculated from the occupancies at α and β sites. In the sample grown with the cooling rate of 0.7 °C/h, the anion displacement parameter of 0.234 was similar to the value used in the calculation of peak area ratio, 0.239.¹⁴ On the other hand, the higher cooling rate of 640 °C/h resulted in a small tetrahedral distortion, which might be attributed to disordering between Zn and Sn.

The relationship between the long-range order parameter and the cooling rate is summarized in [Figure 4](#). The long-range order parameters, calculated from A_{101}/A_{112} and $A_{101}/A_{200\ 004}$, have approximately the same values, and the above experiments and analysis are considered to be valid. From this figure, it was observed that the long-range order parameters from both equation (1) and Rietveld refinement continuously decreased with

the increase of the cooling rate. Generally, in equilibrium states, the order parameter is lower at higher temperatures. It is, thus, qualitatively understood that the states with lower order parameters were frozen in the crystals with higher cooling rates, while the lower cooling rates led to the re-arrangement of atoms during crystal growth.

3.2. Relationship between bandgap and long-range order parameter

The diffuse reflectance spectra of powdered ZnSnP₂ crystals were measured to evaluate the bandgap. The diffuse reflectance, R , is transformed to the Kubelka-Munk function, $F(R)$, by considering the absorption α and the scattering coefficient S .^[24] The bandgap energy, E_g , was evaluated by Tauc's plot of the Kubelka-Munk function based on equation (2),²⁴ where B is the constant.

$$[F(R)E]^2 = \left(\frac{\alpha E}{S}\right)^2 = \left(\frac{B}{S}\right)^2 (E - E_g). \quad (2)$$

Figure 5 shows the Kubelka-Munk function as a function of a photon energy E in every sample. The bandgaps of ZnSnP₂, for the different cooling rates, range from 1.60 to 1.37 eV. As mentioned above, St-Jean *et al.* reported that epitaxially grown ZnSnP₂ on GaAs substrates consisted of both perfectly-ordered and disordered domains.¹³ In this study, the Kubelka-Munk functions continuously shift to lower photon energy with the increase in the cooling rates, as shown in Figure 5b. It is therefore considered that ZnSnP₂ crystals with homogeneous long-range order parameters were obtained. The relationship between

bandgap and long-range order parameter is summarized in [Figure 6](#). In this case, the order parameter calculated from A_{101}/A_{112} was used. The figure shows that the bandgap of ZnSnP_2 crystals decreases, corresponding to the long-range order parameter. In previous work, the bandgap change of ZnSnP_2 through the order-disorder transition has only been discussed qualitatively,¹⁵ however this work provides the quantitative relationship between order parameter and bandgap, which helps understand the phenomena in ZnSnP_2 . In particular, the continuous change of bandgap with long-range order parameter suggests that the crystals obtained in this study were a single phase of chalcopyrite with different long-range order parameters.

3.3. Effect of annealing on ordering behavior and bandgap

We investigated the effect of annealing on ordering behavior using ZnSnP_2 crystals at different temperatures. Table 3 shows the composition of the crystals annealed at different temperatures. The compositions of these samples did not drastically change by the annealing process and these are the near stoichiometric ratio of ZnSnP_2 . Figure 7a shows the powder XRD profiles of the ZnSnP_2 crystals with a cooling rate of $640\text{ }^\circ\text{C/h}$ before and after annealing. The order parameter of this sample was relatively low before annealing. The peak intensities of the superlattice reflection of (101) remained the same at temperatures of 200, 300 and $400\text{ }^\circ\text{C}$ as shown in Figure 7b. Annealing at higher temperatures, such as 500 and $600\text{ }^\circ\text{C}$, led to an increase in the peak intensities of the (101) reflection, which indicated that re-arrangement of Zn and Sn atoms occurred. Although, in general, the long-range order parameter is higher at lower temperatures, it is considered that annealing at lower temperatures made it difficult for the atomic diffusion required for re-arrangement to take place. Small reflection peaks derived from secondary phases such as Sn_4P_3 and $\text{Zn}_2\text{P}_2\text{O}_7$ were observed in the samples annealed at 400 and $500\text{ }^\circ\text{C}$. From the diffuse reflectance spectra, these materials might have no absorption edge in the visible light range and do not influence on the bandgap evaluation.

Similar annealing experiments using the ZnSnP_2 crystals grown with a cooling rate of $0.7\text{ }^\circ\text{C/h}$ were carried out. The powder samples were annealed at temperatures of 650, 670 and $710\text{ }^\circ\text{C}$. As shown in Figures 7c and d, the meaningful change of the peak

intensities from the superlattice reflections is not observed. Considering that the degree of order of the sample with higher order parameter decreases by annealing at near critical temperature, it is thus expected that the critical temperature for the order-disorder transition in ZnSnP_2 does not exist below $700\text{ }^\circ\text{C}$. In previous research, Mughal *et al.* estimated the critical temperature for the order-disorder transition to be about $720\text{ }^\circ\text{C}$ by differential thermal analysis.⁸ However, considering the decomposition temperature of $720\text{ }^\circ\text{C}$,²⁶ they might have confused the decomposition temperature with the order-disorder transition temperature.

The relationship between bandgap and long-range order parameter is summarized in [Figure 8](#), where the curve line is obtained based on the results in [Figure 6](#). In the samples with the cooling rate of $0.7\text{ }^\circ\text{C}/\text{h}$, large shifts in the long-range order parameters were not observed and bandgaps had almost the same values (1.60 eV). In the case of the cooling rate of $640\text{ }^\circ\text{C}/\text{h}$, the increase in long-range order parameter resulted in a change of bandgap from 1.37 to 1.54 eV . In addition, the relationship between bandgap and long-range order parameter was plotted close to the curve line, which indicates that the bandgap of the ZnSnP_2 crystals is defined by the long-range order parameter.

From these experiments, it was clarified that the bandgaps of ZnSnP_2 crystals with lower long-range order parameters can be controlled by increasing the long-range order parameter using an annealing process. In contrast, bandgap tuning might be difficult in the samples with the higher long-range order parameter because the critical temperature

for the order-disorder transition does not exist below the decomposition temperature.

4. Conclusions

In this study, the quantitative evaluation of the long-range order parameter of ZnSnP_2 was carried out, using bulk crystals grown by the flux method with various cooling rates. The area ratio of the superlattice to fundamental reflections in XRD profiles was used for the evaluation and the long-range order parameter was obtained by comparing the measured ratio to the calculated value. From this analysis, it was confirmed that the long-range order parameter of the ZnSnP_2 crystals continuously decreased from 0.94 to 0.54 with the increase of the cooling rate. The similar trend was also obtained from Rietveld refinement. These experimental results can be interpreted as the meaning that the states with lower long-range order parameter were frozen, in the case of the high cooling rates. Furthermore, it was observed that the bandgap of the ZnSnP_2 crystals decreases from 1.60 to 1.37 eV corresponding to the decrease of the long-range order parameter. This study experimentally shows the quantitative relationship between bandgap and long-range order parameter. It was also revealed that the annealing treatment at around 600 °C promoted the rearrangement of cations and increased the long-range order parameter, as well as the bandgap. This fact indicates that bandgap can be controlled by controlling long-range order parameter. However, it was difficult to decrease the long-range order parameter and the bandgap by annealing process, which indicates that the critical temperature for the order-disorder transition does not exist below the decomposition temperature of ZnSnP_2 . The results in this study show that properties in semiconductors are related to the order parameter, which is one of techniques to control properties.

Acknowledgements

The authors wish to thank Ms. C. Harada at Kyoto University for ICP-AES measurements. This work was partly supported by the JST PRESTO program, JSPS KAKENHI Grant Number 26289279 and Grant-in-Aid for JSPS Research Fellow Number 16J09443.

References

- (1) Niki, S.; Contreas, M.; Repins, I.; Powalla, M.; Kushiya, K.; Ishizuka, S.; Matsubara, K. CIGS Absorbers and Processes. *Prog. Photovolt: Res. Appl.* **2010**, *18*, 453–466.
- (2) Takamoto, T.; Kaneiwa, M.; Imaizumi, M.; Yamaguchi, M. InGaP/GaAs-based Multijunction Solar Cells. *Prog. Photovolt: Res. Appl.* **2005**, *13*, 495–511.
- (3) Schorr, S.; Geandier, G. In-situ Investigation of the Temperature Dependent Structural Phase Transition in CuInSe₂ by Synchrotron Radiation. *Cryst. Res. Technol.* **2006**, *41*, 450–457.
- (4) Binsma, J. J. M.; Giling L. J.; Bloem, J. Phase Relations in the System Cu₂S–In₂S₃. *J. Cryst. Growth* **1980**, *50*, 429–436.
- (5) Kumagai, Y.; Choi, M.; Nose, Y.; Oba, F. First-Principles Study of Point Defects in Chalcopyrite ZnSnP₂. *Phys. Rev. B* **2014**, *90*, 125202.
- (6) Shay, J. L.; Wernick, J. H. *Ternary Chalcopyrite Semiconductors: Growth, Electronic Properties, and Applications*; Pergamon Press: Oxford, England, 1975.
- (7) Yokoyama, T.; Oba, F.; Seko, A.; Hayashi, H.; Nose, Y.; Tanaka, I. Theoretical Photovoltaic Conversion Efficiencies of ZnSnP₂, CdSnP₂, and Zn_{1-x}Cd_xSnP₂ Alloys. *Appl. Phys. Express* **2013**, *6*, 061201.
- (8) Mughal, S. A.; Payne, A. J.; Ray, B. Preparation and Phase Studies of the Ternary Semiconducting Compounds ZnSnP₂, ZnGeP₂, ZnSiP₂, CdGeP₂, and CdSiP₂. *J. Mater. Sci.* **1969**, *4*, 895–901.
- (9) Scanlon, D. O.; Walsh, A. Bandgap Engineering of ZnSnP₂ for High-Efficiency Solar Cells. *Appl. Phys. Lett.* **2012**, *100*, 251911.
- (10) Seryogin, G. A.; Nikishin, S. A.; Temkin, H.; Mintairov, A. M.; Merz, J. L.; Holtz,

- M. Order–Disorder Transition in Epitaxial ZnSnP₂. *Appl. Phys. Lett.* **1999**, 74, 2128–2130.
- (11) Francoeur, S.; Seryogin, G. A.; Nikishin, S. A.; Temkin, H. X-ray Diffraction Study of Chalcopyrite Ordering in Epitaxial ZnSnP₂ Grown on GaAs. *Appl. Phys. Lett.* **1999**, 74, 3678–3680.
- (12) Francoeur, S.; Seryogin, G. A.; Nikishin, S. A.; Temkin, H. Quantitative Determination of the Order Parameter in Epitaxial Layers of ZnSnP₂. *Appl. Phys. Lett.* **2000**, 76, 2017–2019.
- (13) St-Jean, P.; Seryogin, G. A.; Francoeur, S. Band Gap of Sphalerite and Chalcopyrite Phases of Epitaxial ZnSnP₂. *Appl. Phys. Lett.* **2010**, 96, 231913.
- (14) Vaipolin, A. A.; Goryunova, N. A.; Kleshchinskii, L. I.; Loshakova, G. V.; Osmanov, E. O. The Structure and Properties of the Semiconducting Compound ZnSnP₂. *Phys. Status Solidi*, **1968**, 29, 435–442.
- (15) Ryan, M. A.; Peterson, M. W.; Williamson, D. L.; Frey, J. S.; Maciel, G. E.; Parkinson, B. A. Metal Site Disorder in Zinc Tin Phosphide. *J. Mater. Res.* **1987**, 2, 528–537.
- (16) Nakatsuka, S.; Nakamoto, H.; Nose, Y.; Uda, T.; Shirai, Y. Bulk Crystal Growth and Characterization of ZnSnP₂ Compound Semiconductor by Flux Method. *Phys. Status Solidi C* **2015** 12, 520–523.
- (17) Izumi, F.; Momma, K. Three-Dimensional Visualization in Powder Diffraction. *Solid State Phenom.* **2007**, 130, 15–20.
- (18) Warren B. E. *X-ray diffraction*; Dover Publications: New York, United States of America, 1969.
- (19) Momma, K.; Izumi, F. VESTA 3 for Three-Dimensional Visualization of Crystal,

- Volumetric and Morphology Data. *J. Appl. Crystallogr.* **2011**, 44, 1272–1276.
- (20) Chantler, C. T. Theoretical Form Factor, Attenuation, and Scattering Tabulation for $Z=1-92$ from $E=1-10$ eV to $E=0.4-1.0$ MeV. *J. Phys. Chem. Ref. Data* **1995**, 24, 71–643.
- (21) Chantler, C. T. Detailed Tabulation of Atomic Form Factors, Photoelectric Absorption and Scattering Cross Section, and Mass Attenuation Coefficients in the Vicinity of Absorption Edges in the Soft X-Ray ($Z=30-36$, $Z=60-89$, $E=0.1$ keV–10 keV), Addressing Convergence Issues of Earlier Work. *J. Phys. Chem. Ref. Data* **2000**, 29, 597–1056.
- (22) Waasmaier, D.; Kirfel, A. New Analytical Scattering-Factor Functions for Free Atoms and Ions. *Acta Crystallogr., Sect. A: Found. Crystallogr.* **1995**, 51, 416–431.
- (23) Neumann, H.; Łażewski, J.; Jochym, P. T.; Parlinski, K. Ab Initio Heat Capacity and Atomic Temperature Factors of Chalcopyrites. *Phy. Rev. B* **2007**, 75, 224301.
- (24) Lin, H.; Huang, C. P.; Li, W.; Ni, C.; S. Shah, S. I.; Tseng, Y. Size Dependency of Nanocrystalline TiO_2 on its Optical Property and Photocatalytic Reactivity Exemplified by 2-Chlorophenol. *Appl. Catal. B* **2006**, 68, 1–11.
- (25) Tauc, J.; Grigorovici, R.; Vancu, A. Optical Properties and Electronic Structure of Amorphous Germanium. *Phys. Status Solidi* **1966**, 15, 627–637.
- (26) Nose, Y.; Uda, T. In *Technical Digest of the 21st International Photovoltaic Science and Engineering Conference (PVSEC-21)*, Fukuoka, 2011; 2D-3P-35.

Tables

Table 1. Compositions of crystals grown by various cooling rates.

Cooling rate / °C h ⁻¹	Composition / at. %			Zn/Sn
	Zn	Sn	P	
0.7	25.6±0.3	25.5±0.5	48.9±0.8	1.00±0.03
15	25.8±0.6	24.9±0.5	49.3±1.3	1.03±0.02
50	26.2±0.8	24.6±0.6	49.2±1.6	1.06±0.03
200	25.8±0.9	25.2±0.6	49.0±1.6	1.02±0.03
640	25.9±0.7	25.0±0.7	49.1±1.4	1.03±0.03

Table 2. Structure parameter refined by Rietveld analysis.

Cooling rate / °C h ⁻¹	Lattice constant / Å		Anion displacement parameter, <i>u</i>	Occupancy, <i>r</i>				Long-range order parameter, η
	<i>a</i>	<i>c</i>		r_{Zn}^{Zn}	r_{Zn}^{Sn}	r_{Sn}^{Sn}	r_{Sn}^{Zn}	
0.7	5.626 ± 0.020	11.252 ± 0.040	0.234 ± 0.001	0.984 ± 0.002	0.016 ± 0.002	0.016 ± 0.002	0.984 ± 0.002	0.968 ± 0.003
15	5.663 ± 0.018	11.326 ± 0.036	0.232 ± 0.001	0.950 ± 0.003	0.050 ± 0.003	0.0500 ± 0.003	0.950 ± 0.003	0.899 ± 0.004
50	5.682 ± 0.023	11.364 ± 0.045	0.234 ± 0.001	0.914 ± 0.003	0.086 ± 0.003	0.086 ± 0.003	0.914 ± 0.003	0.827 ± 0.004
200	5.623 ± 0.017	11.245 ± 0.034	0.236 ± 0.001	0.836 ± 0.004	0.164 ± 0.004	0.164 ± 0.004	0.836 ± 0.004	0.672 ± 0.005
640	5.659 ± 0.012	11.322 ± 0.023	0.248 ± 0.001	0.745 ± 0.004	0.255 ± 0.004	0.255 ± 0.004	0.745 ± 0.004	0.489 ± 0.005

Table 3. Compositions of crystals after annealing process.

Annealing temperature / °C	Crystal grown rate / °C h ⁻¹	Composition / at. %			Zn/Sn
		Zn	Sn	P	
200		25.8 ±0.8	24.9±0.6	49.3±1.4	1.03±0.03
300		26.2±0.5	24.5±0.6	49.3±0.9	1.07±0.03
400	640	25.3±0.6	25.5±0.8	49.2±1.1	0.99±0.03
500		25.2±0.5	26.2±0.4	48.6±0.8	0.96±0.02
600		25.8±0.9	24.8±0.6	49.4±1.3	1.04±0.03
650		26.0 ±0.9	24.7±0.5	49.3±1.9	1.06±0.03
670	0.7	25.6±0.4	25.3±0.9	49.1±1.0	1.01±0.04
710		25.5±0.6	25.4±0.6	49.1±1.1	1.00±0.02

Figure captions

Figure 1. Crystalline structures of ZnSnP_2 with (a) chalcopyrite and (b) sphalerite. The red, blue and green atoms represent Zn, Sn and P, respectively. In the sphalerite structure, Zn and Sn atoms occupy their sites randomly.

Figure 2. (a) Powder XRD profiles of ZnSnP_2 crystals grown with different cooling rates in linear scale and (b) enlarged view of (101) reflection peaks in log scale.

Figure 3. Calculated peak area ratio of A_{101}/A_{112} and $A_{101}/A_{200\ 004}$ as a function of long-range order parameter η .

Figure 4. Relationship between the long-range order parameter η of the ZnSnP_2 crystal and the cooling rates in crystal growth. The triangle and circle symbols represent the η values calculated from A_{101}/A_{112} and $A_{101}/A_{200\ 004}$, respectively. The order parameter obtained from Rietveld refinement is shown by square symbols. The error bar of the long-range order parameter are within the symbol size.

Figure 5. (a) Diffuse reflectance of ZnSnP₂ powder fabricated by the various cooling rates and (b) the Tauc's plot of Kubelka-Munk transform using the diffuse reflectance.

Figure 6. Relationship between bandgap and long-range order parameter in the ZnSnP₂ crystals. The long-range order parameter was calculated using A_{101}/A_{112} . The error bars of the long-range order parameter are within the symbol size.

Figure 7. Influence of the annealing temperatures on the powder XRD profiles of ZnSnP₂ crystals grown by the cooling rate of (a), (b) 640 °C h⁻¹ and (c), (d) 0.7 °C h⁻¹.

Figure 8. Relationship between bandgap and long-range order parameter in ZnSnP₂ crystals before and after annealing. The curve line was obtained based on the analysis of the ZnSnP₂ crystals grown by various cooling rates. The error bars of the long-range order parameter are within the symbol size.

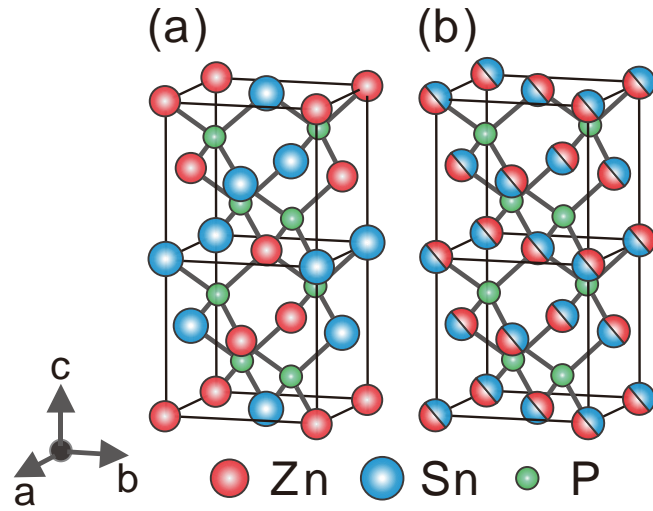


Figure 1. Crystalline structures of ZnSnP_2 with (a) chalcopyrite and (b) sphalerite. The red, blue and green atoms represent Zn, Sn and P, respectively. In the sphalerite structure, Zn and Sn atoms occupy their sites randomly.

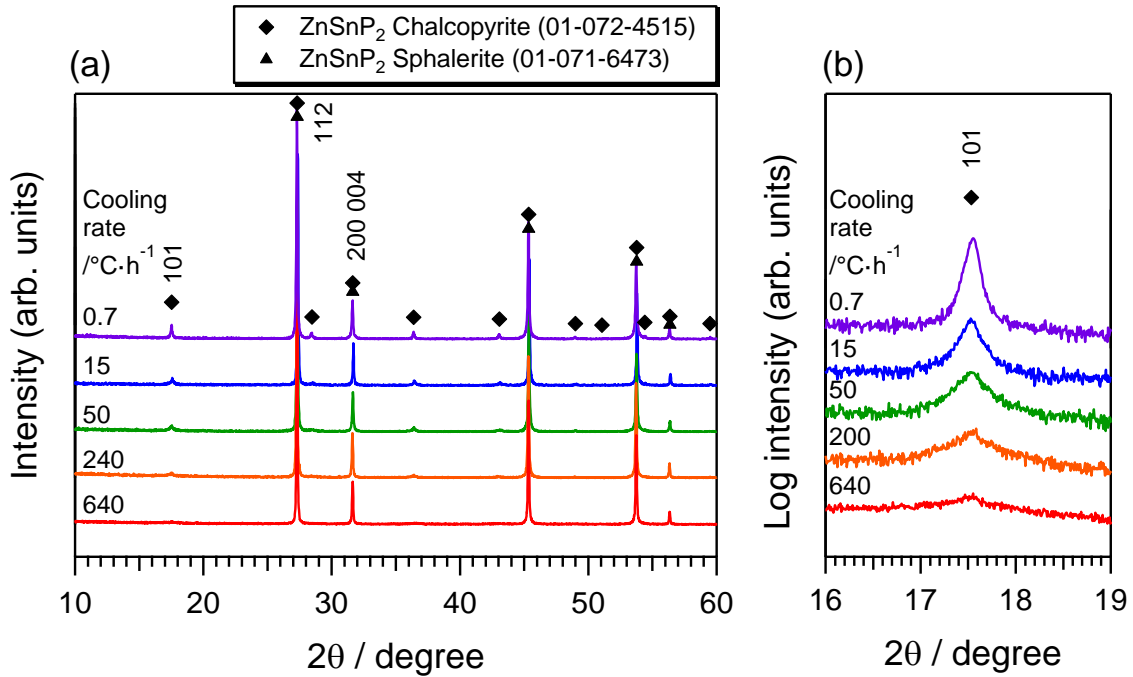


Figure 2. (a) Powder XRD profiles of ZnSnP_2 crystals grown with different cooling rates in linear scale and (b) enlarged view of (101) reflection peaks in log scale.

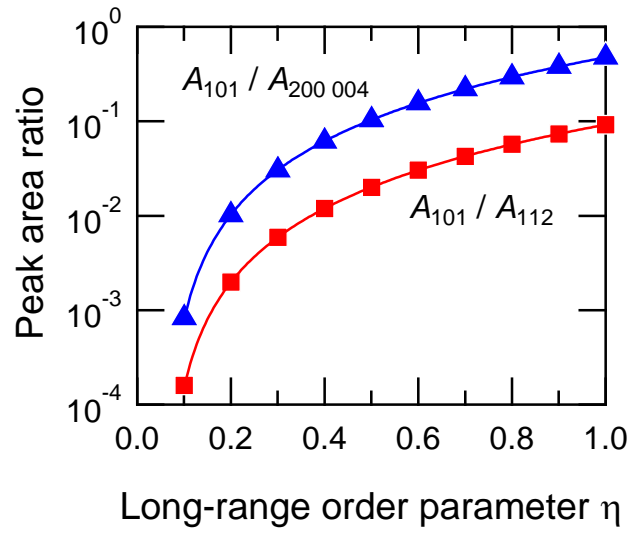


Figure 3. Calculated peak area ratio of A_{101}/A_{112} and $A_{101}/A_{200\ 004}$ as a function of long-range order parameter η .

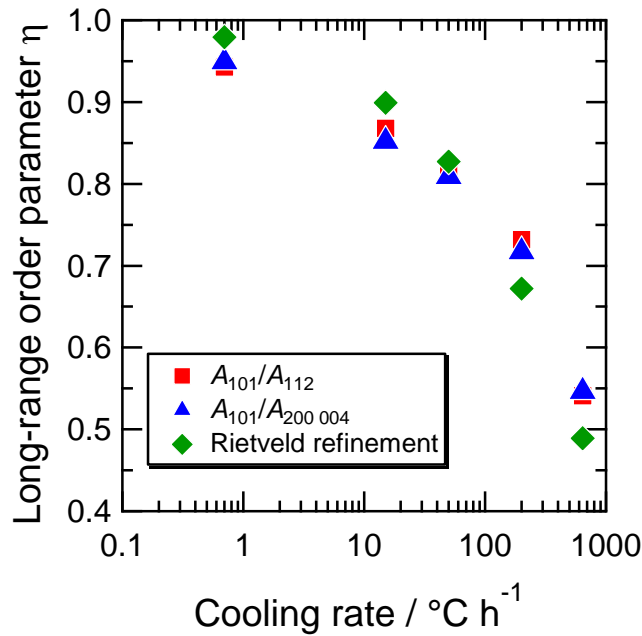


Figure 4. Relationship between the long-range order parameter η of the ZnSnP_2 crystal and the cooling rates in crystal growth. The triangle and circle symbols represent the η values calculated from A_{101}/A_{112} and $A_{101}/A_{200\ 004}$, respectively. The order parameter obtained from Rietveld refinement is shown by square symbols. The error bar of the long-range order parameter are within the symbol size.

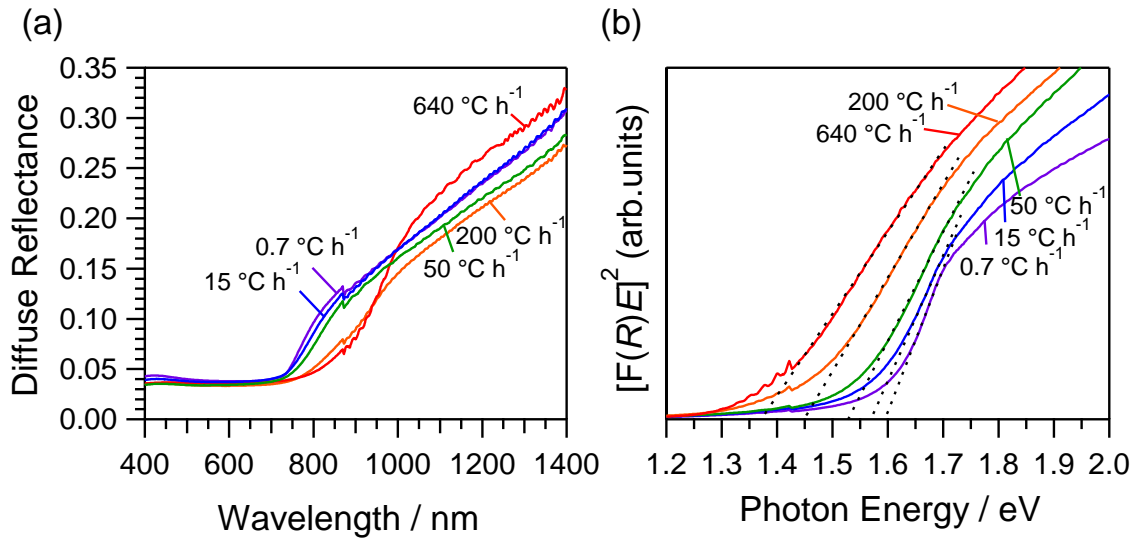


Figure 5. (a) Diffuse reflectance of ZnSnP₂ powder fabricated by the various cooling rates and (b) the Tauc's plot of Kubelka-Munk transform using the diffuse reflectance.

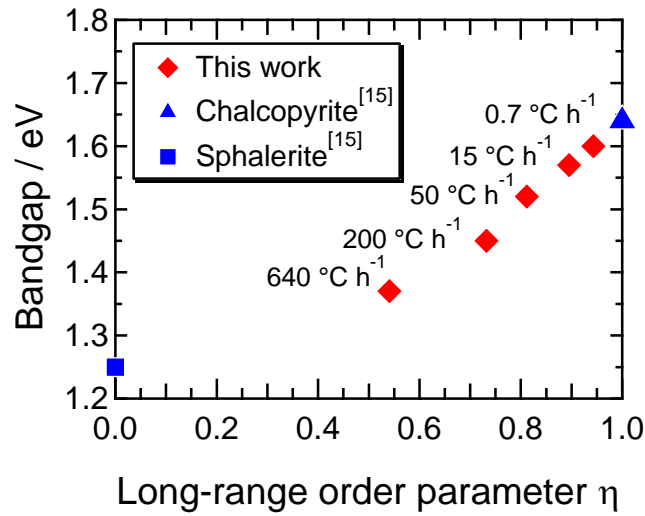


Figure 6. Relationship between bandgap and long-range order parameter in the ZnSnP₂ crystals. The long-range order parameter was calculated using A_{101}/A_{112} . The error bars of the long-range order parameter are within the symbol size.

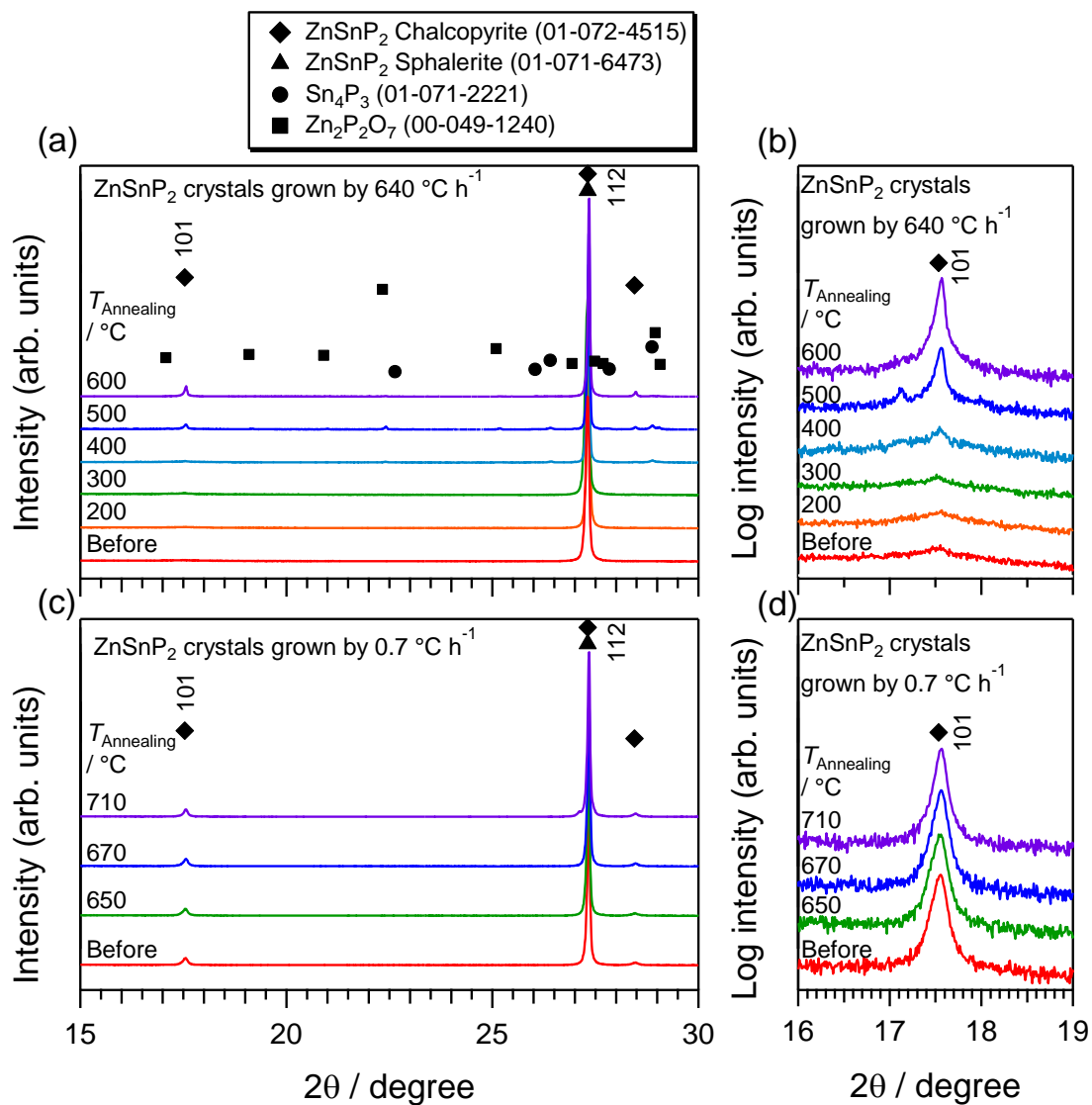


Figure 7. Influence of the annealing temperatures on the powder XRD profiles of ZnSnP₂ crystals grown by the cooling rate of (a), (b) 640 °C h⁻¹ and (c), (d) 0.7 °C h⁻¹.

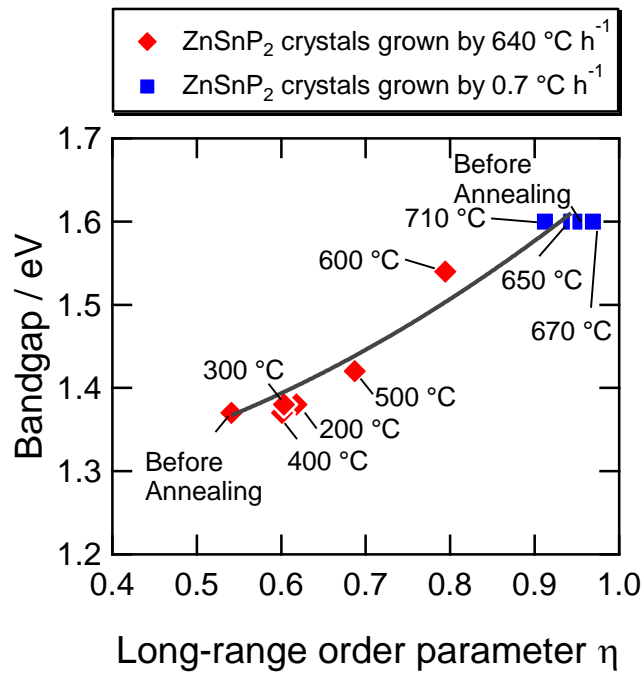


Figure 8. Relationship between bandgap and long-range order parameter in ZnSnP_2 crystals before and after annealing. The curve line was obtained based on the analysis of the ZnSnP_2 crystals grown by various cooling rates. The error bars of the long-range order parameter are within the symbol size.

Table of Contents image

